

Creative Commons Attribution 4.0 International (CC BY 4.0)

<https://creativecommons.org/licenses/by/4.0/>

Access to this work was provided by the University of Maryland, Baltimore County (UMBC) ScholarWorks@UMBC digital repository on the Maryland Shared Open Access (MD-SOAR) platform.

Please provide feedback

Please support the ScholarWorks@UMBC repository by emailing scholarworks-group@umbc.edu and telling us what having access to this work means to you and why it's important to you. Thank you.



Magnetic Field Observations in the Very Local Interstellar Medium by Voyagers 1 and 2

L. F. Burlaga¹ , N. F. Ness⁸, D. B. Berdichevsky^{2,3}, L. K. Jian⁴ , W. Kurth⁵ , J. Park^{4,6} , J. Rankin⁷ , and A. Szabo⁴ ¹Leonard F. Burlaga, Inc., Davidsonville, MD 21035, USA²IFIR/UNR-CONICET, Esmeralda y 27 de Febrero, Rosario, Santa Fe, Argentina; lburlagahsp@verizon.net³Trident, College Park, MD 20740, USA⁴Heliophysics Science Division, NASA/GSFC, Greenbelt, MD 20771, USA⁵Department of Physics and Astronomy, University of Iowa, Iowa City, IA 52242, USA⁶University of Maryland, Baltimore County, Baltimore, MD 21250, USA⁷Department of Astrophysical Sciences, Princeton University, Princeton, NJ 08540, USA

Received 2022 February 21; revised 2022 April 6; accepted 2022 April 6; published 2022 June 15

Abstract

Observations of the magnetic field \mathbf{B} in the very local interstellar medium (VLISM) were made by Voyager 1 (V1) in the northern hemisphere from 2012 to mid-2021 and by Voyager 2 (V2) in the southern hemisphere from 2018 through 2020. Near 2019.4, V2 observed an abrupt increase in B associated with a pressure front near the heliopause. During 2020, V2 observed an abrupt increase in B at a jump in B that was preceded by electron plasma oscillations and cosmic rays, indicating that it was a shock. The shock was followed by a decrease in B ending ~ 50 days later. V2 observed large-scale waves in all three components of \mathbf{B} , before and after the shock. The largest- and intermediate-amplitude waves were in the BN and BR component, respectively, indicating that the waves were predominantly transverse several au from the heliopause. It was shown previously that waves near the heliopause were predominantly longitudinal at V1 and V2. Thus, V2 observed a mode transformation process within 10 au of the heliopause in the southern hemisphere, like that observed by V1 in the northern hemisphere. The elevation and azimuthal angles observed by V1 and V2 varied linearly with increasing distance in the VLISM. Voyager 1 observed jumps in B at two shocks and a pressure front, each followed by a decrease in B in a ramp. V1 also observed a fourth jump in B , at 2020.4, but B continued to increase until at least year 2021.5. This long-lasting increase in B was not anticipated.

Unified Astronomy Thesaurus concepts: [Interstellar magnetic fields \(845\)](#)

1. Introduction

The heliopause is a boundary that separates the heliosheath (that contains magnetic fields and plasmas that originate in the Sun) from the interstellar medium (that contains magnetic fields and particles of stellar/interstellar origin). The interaction of the heliosheath with the very local interstellar medium (VLISM) was discussed by Holzer (1989), Zank (1999, 2015), and Zank et al. (2017). The first indirect evidence of a possible shock in the VLISM was made by Gurnett et al. (1993) using remote radio observations by the PWS experiment on Voyager 1 (V1). Whang & Burlaga (1993) modeled this shock as a spherical shock driven by a global merged interaction region. 3D numerical models of the interaction of the shock with the heliopause were published by Zank & Müller (2003), Washimi et al. (2011, 2017), Fermo et al. (2015), Kim et al. (2017), and Pogorelov et al. (2017a, 2017b). Burlaga & Ness (2016), Burlaga et al. (2019a), and Richardson et al. (2017) discussed two pressure pulses that were presumably transmitted through the heliopause. Observations of the heliopause were first made by particles and fields instruments on the V1 spacecraft, moving away from the Sun in the northern hemisphere. The spacecraft crossed the heliopause on $\approx 2012.65/\text{DOY } 238$ (2012 August 25) at 121.58 au from the Sun near $35^\circ 0$ latitude and 174° longitude in heliographic inertial (HGI) coordinates (Burlaga et al. 2013b, Krimigis et al. 2013;

Stone et al. 2013; Burlaga et al. 2014; Gurnett et al. 2013). The crossing of the heliopause occurred earlier than predicted by Karmesin et al. (1995), Wang & Belcher (1999), Zank & Müller (2003), McComas et al. (2010), Zank (2015), and Pogorelov et al. (2017b). Gurnett et al. (2013) confirmed that V1 crossed the heliopause and entered the interstellar medium.

Voyager 2 (V2) crossed the heliopause in the southern hemisphere near 2018 November 5 at a distance of ≈ 119.0 au at $\approx 32^\circ 2$ below the solar equatorial plane and $218^\circ 3$ in HGI longitude (Burlaga et al. 2019a; Gurnett & Kurth 2019; Krimigis et al. 2019; Richardson et al. 2019 and Stone et al. 2019). The plasma and magnetic fields observed by V2 around the time left the Sun during the late declining phase of solar cycle 24. V2 observed a much thinner and simpler heliopause than V1, as well as stronger interstellar magnetic fields, and it discovered a “magnetic barrier” in the heliosheath adjacent to the heliopause, which strongly influenced the entry of cosmic rays into the heliosphere. The magnetic field direction observed by V2 changed smoothly from the time of arrival of the magnetic barrier at V2, through the magnetic barrier, and through the interstellar medium in 2018, with a small (a few degrees) or no change across the heliopause.

Burlaga et al. (2014) identified *longitudinal* fluctuations among the microscale fluctuations of the hourly averages of the magnetic field \mathbf{B} observed on a scale of 1 day by V1 from 2011.0 to 2012.3143, when it was within the distant heliosheath where the average magnetic field strength $\langle B \rangle = 0.17$ nT. They also observed *longitudinal* fluctuations, during the interval from 2012.6503 to 2013.5855 when V1 was within the *interstellar* plasma where $\langle B \rangle = 0.47$ nT. In both the heliosheath and the VLISM, the fluctuations were primarily longitudinal fluctuations,

⁸ Now retired.

varying along the average \mathbf{B} , which is $\approx T$ -direction in spacecraft-centered radial–tangential–normal (RTN) coordinates.

V1 continued to observe *longitudinal* magnetic field fluctuations in the VLISM between 124.14 and 128.71 au at 34.6°N ($\sim 2\text{--}7$ au upwind of the heliopause) from 2013/DAY 133 to 2014/DAY 235 (Burlaga et al. 2015). V1 observed *transverse* (Alfvénic) fluctuations of B between 131.40 and 135.98 au at latitudes $34.6^\circ\text{--}34.7^\circ\text{N}$ ($\sim 10\text{--}14$ au beyond the heliopause) from 2015/DOY 145 to 2016/DOY 248 (Burlaga et al. 2018). The most recent V1 observations continued to show the presence of transverse fluctuations of B in the VLISM from 141.44 to 146.01 au at $34.7^\circ\text{--}34.8^\circ\text{N}$ ($\sim 20\text{--}24$ au from the heliopause) between 2018/DOY 5 and 2019/DOY 178 (Burlaga et al. 2020b).

Zank et al. (2017) developed an interpretation that only compressible fast magnetosonic modes can be transmitted from the inner heliosheath across the heliopause and into the VLISM, thus providing an explanation for the observations of Burlaga et al. (2014, 2015). Zank et al. (2019) proposed the theoretical possibility that a low plasma beta VLISM admits three-wave interactions that undergo mode conversion decaying into Alfvén waves. Zank et al. (2019) estimated that compressible fast modes are fully converted into incompressible fluctuations within ~ 10 au of the heliopause, which is consistent with the V1 observations and with the V2 observations that will be discussed below.

V2 crossed the heliopause in 2018/DOY 309, and as will be shown in this paper, it also continued to observe longitudinal magnetic field fluctuations nearly along the average magnetic field direction in the VLISM at distances from 119.00 to 121.48 au and latitudes from 32.2° to 32.4°S from 2018 day 309 to 2019 day 230 (Burlaga et al. 2020a). This result confirms the V1 observations of Burlaga et al. (2015) of a longitudinal magnetic field immediately beyond the heliopause and the conversion to transverse (Alfvénic) waves within 10 au of the heliopause.

Intermittency in the fluctuations of \mathbf{B} (which might be an indication of turbulence on larger scales), since was observed by V1 and V2 after they crossed the heliopause (Burlaga et al. 2014, 2015, 2018; Zhao et al. 2020). In this paper, we use the kurtosis to identify and characterize the intermittency observed by V2 in the VLISM. In the RTN coordinate system, \mathbf{R} is the unit radius vector directed radially from the Sun, \mathbf{T} is the cross-product of the solar rotation vector with \mathbf{R} , and the unit vector \mathbf{N} completes a right-handed system. The azimuthal angle λ is in the $\mathbf{R}\text{--}\mathbf{T}$ plane, and it is 0° when \mathbf{B} points in the radial outward direction. The elevation angle δ is zero when \mathbf{B} is in the $\mathbf{R}\text{--}\mathbf{T}$ plane.

In the VLISM explored to date, from 2012 to mid-2021, V1 observed four maxima in B associated with “jumps” (abrupt increases) in the magnetic field strength B . The first two jumps were associated with shock waves (Burlaga & Ness 2016; Burlaga et al. 2021). Gurnett et al. (2013) demonstrated that V1 was indeed in the VLISM.

However, the shocks were 10^4 times thicker than the collisionless shocks near 1 au! Mostafavi & Zank (2018a, 2018b) argued theoretically that shock waves in the very low density VLISM are collisional shocks associated with resistivity and viscosity. The latter two jumps observed by V1 were not associated with plasma oscillations and electron beams, and they were much broader than the two shocks, so they were attributed to the passage of pressure fronts by

Burlaga et al. (2021). Each of the jumps associated with shocks and the pressure front pf1 was followed by the slow decline to lower magnetic field strengths. The most recent observations of the magnetic field in the VLISM, presented in this paper, show that B continued to *increase* behind the last observed jump pf2 for ~ 1 yr. This is a surprising and significant observation that was not predicted.

Calibration of the magnetometers that provided the data for this paper has been a complicated and evolving process because the spacecraft have been operating since 1977. The initial mission was to study Jupiter and Saturn, with the hope that the spacecraft could ultimately fly past Uranus and Neptune. The initial design of the magnetic field experiment is described by Behannon et al. (1977). In fact, both spacecraft have explored the heliosheath and are currently exploring the interstellar medium. The magnetometers were not designed for such a mission, and there were no expectations of reaching beyond the heliopause and out to ~ 150 au, which is the present distance of V1. The coinvestigators M. Acuña and L. Burlaga updated the calibration methods for many years, and Berdichevsky (2009) and Berdichevsky (2015), as well as Jeewoo Park (private communication), developed the calibration techniques that evolved during the most recent years.

2. Voyager 2 Observations

2.1. Voyager 2 Observations near the Heliopause

An overview of the V2 observations from 2018 through 2020 is shown in Figure 1. This figure includes results presented previously by Burlaga et al. (2019b) and Burlaga et al. (2020a) obtained out to 121.48 au at 2019.63. The results in the paper include (1) heliosheath observations with weak magnetic field strengths and a “sector structure” in λ (but with large elevation angles δ , which are not commonly seen at 1 au), (2) a magnetic barrier between about 2018.63 and 2018.85, (3) the heliopause that was crossed on 2018.85, and (4) an exponential decay in B beyond the heliopause ending at approximately 2019.4. Note that the heliopause crossing was marked by a nearly discontinuous increase in the magnetic field strength B on day 309 (Burlaga et al. 2019b). Other aspects of the heliopause crossing were discussed by Krimigis et al. (2019), Richardson et al. (2019), and Stone et al. (2019).

Figure 1 shows the existence of a “rotation region” in which the direction of the magnetic field, given by the azimuthal direction $\lambda(t)$ and elevation angle $\delta(t)$, changed significantly. The rotation region began at the vertical line “A” at ~ 2018.59 when the spacecraft entered the magnetic barrier (Pogorelov et al. 2017a, 2017b; Washimi et al. 2011); it continued through the magnetic barrier, then it moved across the thin heliopause at ~ 2018.85 with no visible change in direction, and continued in the VLISM past the heliopause until ~ 2018.92 , which is marked by the vertical line “B.” Assuming that the magnetic barrier and heliopause were stationary, the spacecraft moved through the rotation region in ~ 128 days with a speed of 15.3 km s^{-1} , so the thickness of rotation region was $\sim 1.59 \times 10^8\text{ km}$. The azimuthal angle decreased smoothly from $\sim 293^\circ$ to $\sim 266^\circ$, while the elevation angle increased from $\sim -45^\circ$ to $\sim 23^\circ$. The magnetic field strength increased significantly in the magnetic barrier, while the direction of \mathbf{B} also changed significantly, but there was no change in the direction of \mathbf{B} across the relatively thin heliopause. The average magnetic field strength in the rotation region $\langle B \rangle$ was 0.377 nT. The

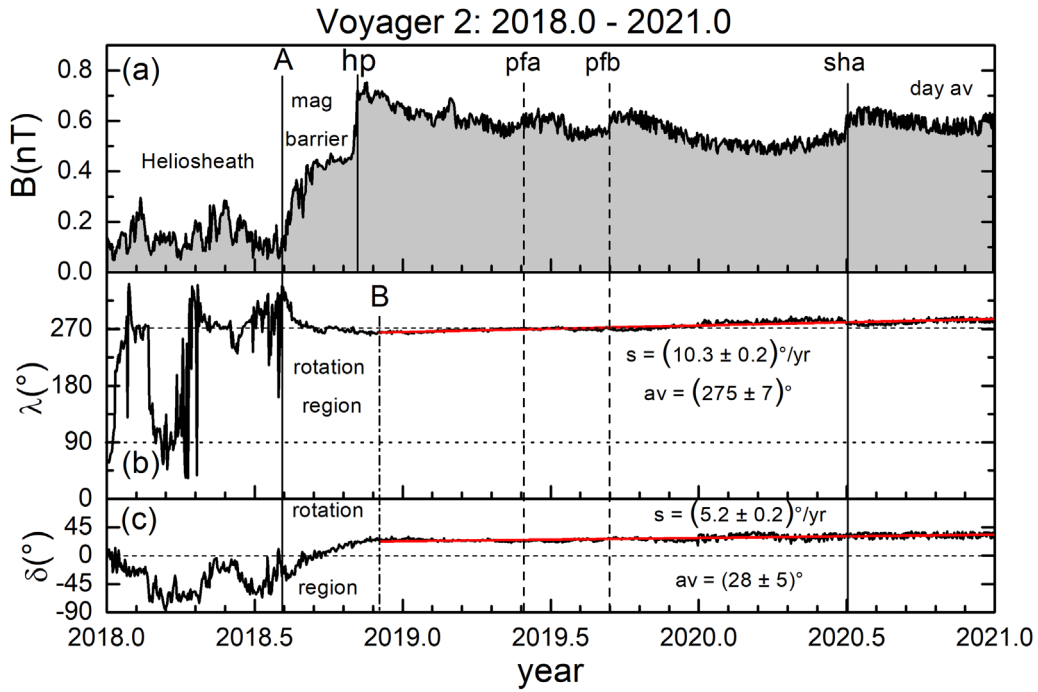


Figure 1. V2 observations from 2018.0 to 2021.0. (a) The magnetic field strength B vs. time. The figure begins with observations made in the heliosheath, where the magnetic field strength B is weak. On approximately 2018.6 V2 entered the magnetic barrier and a “rotation region” at the time of line “A.” It moved through the magnetic barrier until it reached the heliopause (HP). The spacecraft then moved through the VLISM until it crossed two small jumps (increases) in B , pfa and pfb, and then crossed a shock (sha) on 2020.5. (b) This panel shows the azimuthal angle, λ , as a function of time. Initially, V2 moved through the outermost regions of the heliosheath, where it crossed a “sector” in which λ changed from 270° to approximately 90° and then returned to nearly 270° . V2 entered the rotation region (line A), passed through the heliopause (with essentially no change in direction), and moved beyond the heliopause until it crossed the vertical line “B” near the end of 2018. After that, the azimuthal angle λ increased linearly and slowly until the end of the year. λ decreased from $\sim 315^\circ$ to $\sim 270^\circ$ in 2018. The azimuthal angle δ shown in panel (c) behaved qualitatively like λ .

average unit vector of the magnetic field was $\mathbf{B}/\langle B \rangle = 0.021\mathbf{R} - 0.905\mathbf{T} + 0.127\mathbf{N}$ in the spacecraft-centered RTN coordinate system. Thus, the variation of $\mathbf{B}/\langle B \rangle$ was primarily in the \mathbf{T} – \mathbf{N} plane because the radial component was very small. The angle between the average magnetic field and the radial direction \mathbf{R} in the rotation region was $\cos^{-1}(0.021) = 89^\circ$. Thus, the average magnetic field in the rotation region was orthogonal to the radial direction in the spacecraft-centered RTN coordinate system. Since the latitude of V2 was -32° , the normal to the plane of rotation was $\sim -32^\circ$ in heliographic inertial coordinates. Since the heliopause was embedded in the rotation region, the normal to the heliopause was likewise directed radially $\sim -32^\circ$ from the ecliptic at the location of V2.

2.2. Direction of the Interstellar Magnetic Field Observed by Voyager 2

Beyond the rotation region discussed above, i.e., in the VLISM beyond dotted–dashed line “B” at approximately 2018.92 shown in Figures 1(b) and (c), the angles λ and δ increased linearly, but slowly, with increasing distance and time, from ~ 2018.92 until the end of 2020, which is the extent of the current data (Figure 1). The slope of the azimuthal angle was $s_\lambda = 10.3 \pm 0.2 \text{ yr}^{-1}$, and the average elevation angle was $s_\delta = 5.2 \pm 0.2 \text{ yr}^{-1}$. The average azimuthal angle between 2018.92 and 2021.0 was $275^\circ \pm 7^\circ$, and the average elevation angle during the same interval was $28^\circ \pm 5^\circ$. Thus, the direction of the magnetic field observed by V2 beyond the heliopause in the southern hemisphere was coincidentally close to the Parker spiral magnetic field direction (Parker 1958, 1961). A similar linear increase of the magnetic field directions

λ and δ has been observed by V1 as the spacecraft moved through a very thick “boundary layer” (Pogorelov et al. 2009) in the VLISM.

Immediately after crossing the heliopause at 119.0 au until at least 2019 day 230, when V2 was at 121.5, 2.5 au from the heliopause, V2 was observing primarily longitudinal fluctuations (Burlaga et al. 2020a). This result supports the hypothesis of Burlaga et al. (2014) and the results of Burlaga et al. (2015), based on V1 observations, which showed that longitudinal fluctuations can propagate from the heliosheath, through the heliopause, and into the VLISM for a distance of several au. We shall examine the evolution of the magnetic field fluctuations beyond this distance in the new data.

3. “Jumps,” Fluctuations, and Waves in the Magnetic Field Observed by Voyager 2

3.1. Two Jump-ramp Events in the VLISM Beyond the Heliopause

Beyond the heliopause, V2 observed three “jumps” (abrupt increases) in B labeled “pfa,” “pfb,” and “sha,” shown in Figure 1. Each rapid jump in B was followed by a slow decrease in B that we refer to as a “ramp.” This section considers only “pfb” and “sha.” The difference between these events is discussed in the following paragraph, and the remainder of the section discusses “pfb” in detail. A detailed discussion of event “sha” is presented in Section 3.2.

Figure 2(a) shows the jump in B associated with the pressure front pfb just after 2019–244, which was followed by a “ramp.” Later, V2 observed a second jump in B that was followed by a similar ramp in which B decreased slowly. The lower

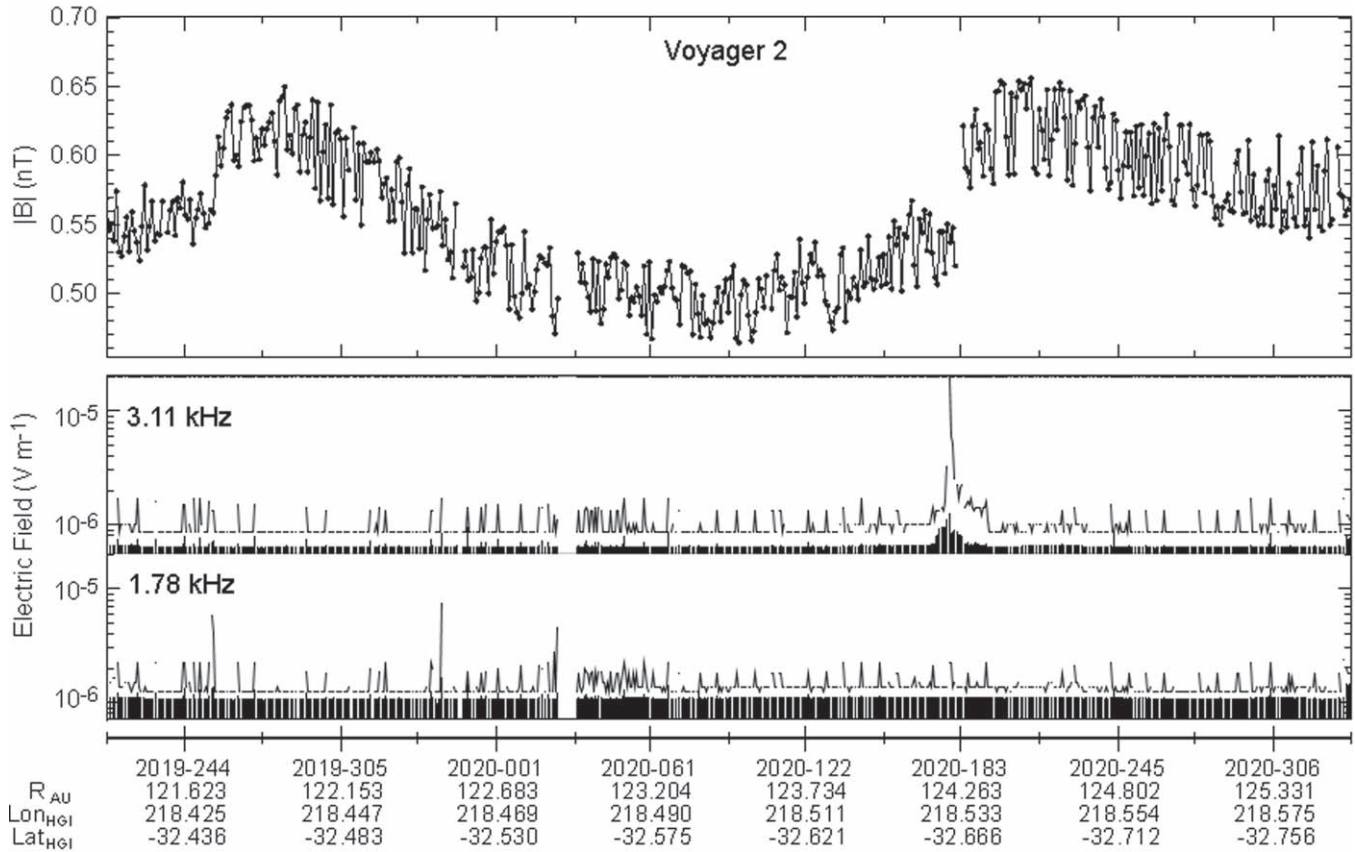


Figure 2. The top panel shows a jump-ramp structure (pfb) on the left followed by a second jump-ramp structure (sha) on the right. The middle panel shows a spike in the 3.11 kHz electric field that was associated with electron plasma oscillations ahead of the jump sha. This is a strong indication that the jump in B was a shock that accelerated an electron beam that generated electron plasma oscillations.

two panels of Figure 2 show the electric field at 3.1 kHz (Figure 2(b)) and at 1.78 kHz (Figure 2(c)). In panels (b) and (c), the variation in electric field strength in two of the plasma wave science (PWS) spectrum analyzer channels (1.78 and 3.11 kHz) is plotted. The solid black areas represent the average, while the line above is the peak amplitude for each averaging interval. For most of this time interval, the peaks are responding to variations in a multiplexor in the V2 flight data system that failed a few months after launch. Voltages on other inputs to this multiplexor can affect the value returned when the PWS spectrum analyzer channels are selected. These interfering signals are typically identified by appearing in all upper eight spectrum analyzer channels (from 1.0 to 56.2 kHz) simultaneously. Only the signals in the 3.11 kHz channel between \sim day 171 and 193 are thought to be valid, natural signals. The distinguishing feature between the two jump-ramp structures is the peak in the electric field at 3.11 kHz preceding the second jump in B near 2020-183 that is not present at pfb.

3.2. The Pressure Front pfb

The jump-ramp structure of the pressure front is shown by the profile of the magnetic field strength from 2019 day \sim 230 to day 350 in Figure 3(a). The data in the plot are 1 day averages of the magnetic field. As described above, pfb shows no evidence for electron plasma oscillations ahead of the jump in B , which is why we identified it as a pressure front rather than a shock.

The jump in B is shown by the red curve in Figure 3(a), which was computed using a sigmoid/Boltzmann curve, namely, $y = B + (B_1 - B_2)/(1 + \exp((\text{doy} - \text{doy}_0)/d))$. Fitting the observations with this curve gives $B_1 = 0.556 \pm 0.003$ nT before the jump and $B_2 = 0.618 \pm 0.002$ nT after the jump, hence $B_2/B_1 = 1.11$. This 11% increase in B occurred over an interval of ~ 7 days. The jump pfb occurred on day \sim 258 at ~ 121.7 au, which was ~ 2.7 au beyond the heliopause crossing at 119 au.

The passage time was comparable to that of the two probable shocks observed by V1 on 2012.92330 (2012/DOY 335; Burlaga et al. 2013b; Gurnett et al. 2013) and the second shock on 2014.6438 (2014/DOY 236; Gurnett et al. 2015; Burlaga & Ness 2016). The azimuthal angle λ in panel (b) and elevation angle δ in panel (c) in Figure 3 show that the direction of the magnetic field did not change across the jump in B . In fact, the angles were essentially constant throughout the interval from 2019 day 230 to day 350, with mean values $\lambda = 271^\circ \pm 2^\circ$ and $\delta = 25^\circ \pm 2^\circ$.

The ramp following the jump in B , extending from day 260 to day 350, is shown by the 48 s averages of the magnetic field in Figure 3(a). There is some indication that there are fluctuations in B in the ramp, but we shall not analyze them in detail. Similar fluctuations have been observed at pf1 by Burlaga et al. (2019a). The ramp associated with pfb is shown in more detail in Figure 4, which plots 1 day averages of B and the components $-BT$, BN , and BR in panels (a), (b), (c), and (d) respectively. Note that the axes were chosen so that each panel

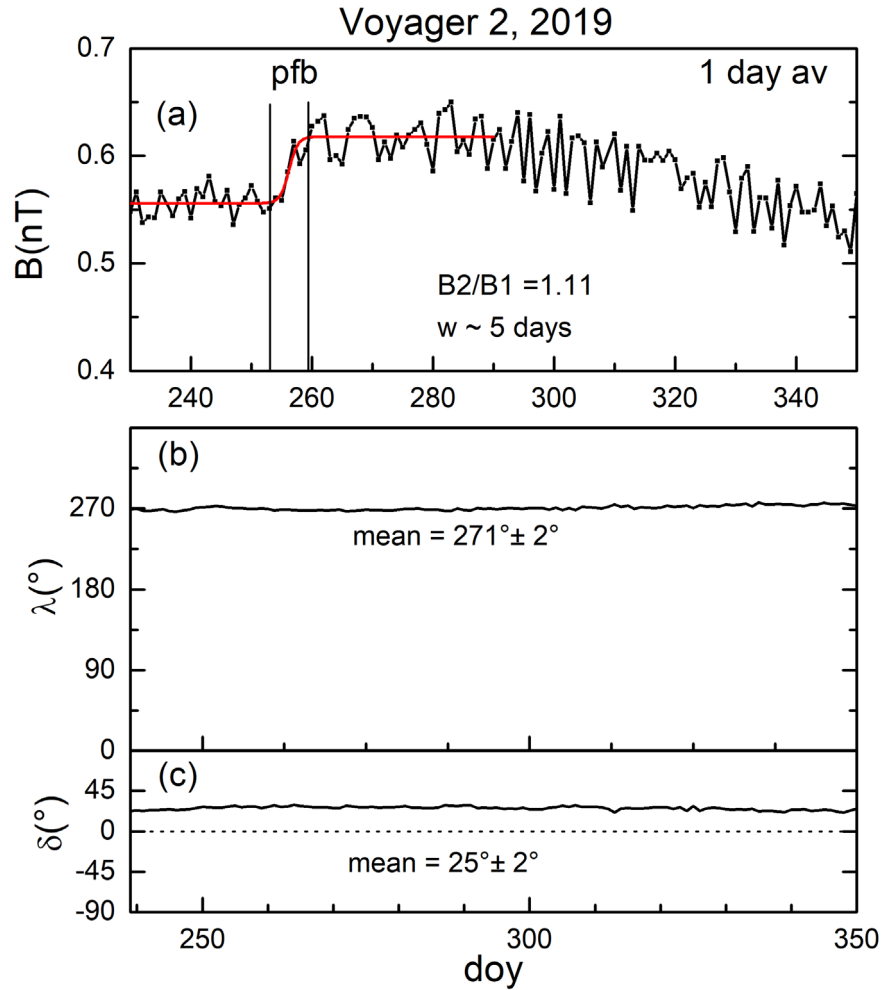


Figure 3. Panel (a) shows 48 s averages of B vs. day of year in 2019. The dominant feature is the jump in B , marked by the interval “pfb” in which the ratio of the magnetic field strength after the jump to that before the jump was $B_2/B_1 = 1.11$. V2 moved through the jump in ~ 7 days. The azimuthal angle λ and the elevation angle δ in panels (b) and (c), respectively, did not change across the jump. The azimuthal and elevation angles remained nearly constant from day 238 through day 350, with the mean values $\lambda = 271^\circ \pm 2^\circ$ and $\delta = 25^\circ \pm 2^\circ$, respectively.

covers the same range for the associated magnetic field component, but the initial value is different in each panel. The ramp is described to good approximation by cubic polynomials for B and each of the components, which are as shown by the red curves following the jump in B .

The 1 day observations scatter about the curves for each of the components. The standard deviation (SD) of the points above the curve describing $B(t)$ is largest, $SD = 0.042$ nT, because it includes the fluctuations from all of the components. One can see by inspection that the scatter is smallest for the BR component; the standard deviation of the points about the curve is $SD = 0.025$ nT. The standard deviations measuring the larger scatter of the points associated with the BN and $-BT$ components are the same, $SD = 0.034$ nT.

The relatively large fluctuations in the BT component (nearly along the T -direction in the ramp) correspond to longitudinal fluctuations, since BT was within $\sim 25^\circ$ of the average magnetic field in the VLISM. The fluctuations in the BN component were equally large. However, the BN component of B was perpendicular to the T , i.e., the BN component corresponds to a transverse fluctuation. Thus, V2 observed “mixed” fluctuations in the ramp of pfb, with comparable longitude fluctuations ($-BT$) and transverse fluctuations (BN) between 2.5 and 3.5 au beyond the heliopause.

3.3. Magnetic Fields and Fluctuations Associated with a Shock Observed by Voyager 2 during 2020

As we discussed in Section 3.1, V2 observed a third jump in B , in 2020 at 124 au. The magnitude of B of this jump and the angles λ and δ are plotted in Figures 5(a), (b), and (c), respectively, during the interval from day 100 through day 350.

Figure 6 shows that this jump in B was associated with a shock, “sha.” This event was first reported by Gurnett & Kurth (2019). They identified the larger amplitudes and accompanying fluctuations as evidence for plasma oscillations. Weaker signals with lower levels of fluctuations prior to day 176 were interpreted as radio emissions. The ratio of the response in the 1.78 and 3.11 kHz channels near the peak of the event, along with the frequency response curves for these two channels, was used to narrow the frequency of the emission to ~ 2.65 kHz. The existence of the plasma oscillations provides a strong argument for the shock interpretation for the “sh” event, since it is assumed that the bursty intermissions are driven by low-energy electrons in an electron foreshock associated with a nearby shock. The plasma oscillations peaked late on day 178. There was a decrease in amplitude followed by continuing weak emissions until day 193. Previous observations (e.g., Burlaga et al. 2013a) showed that the plasma oscillations

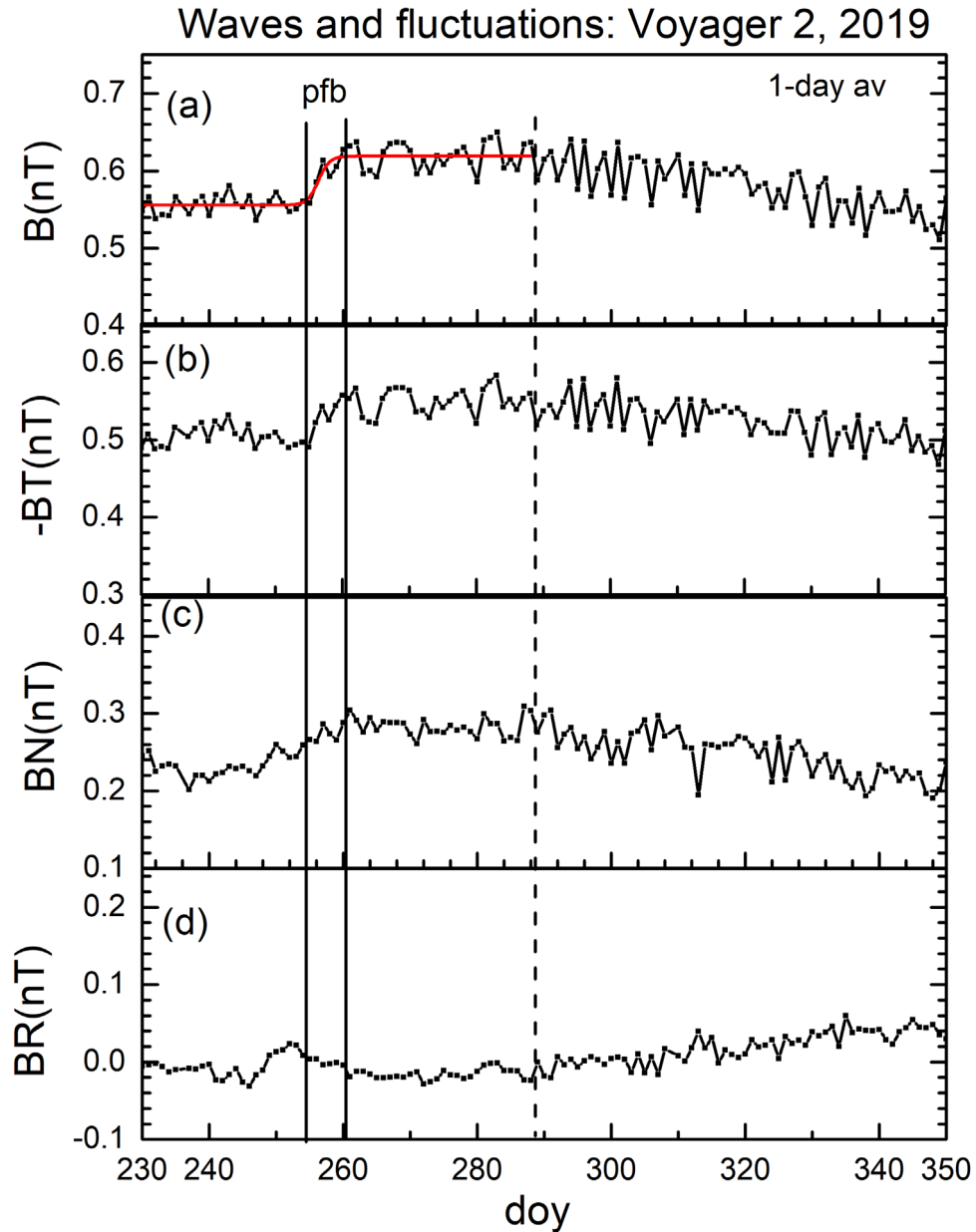


Figure 4. This figure shows hour averages of the jump pfb (panel (a)), as well as the components $-BT$ (panel (b)), BN (panel (c)), and BR (panel (d)). The standard deviations following the jump in B are shown in each panel.

ceased near the time that a shock passed over the spacecraft. If the increase in amplitude between days 182 and 183 marks a transition from local plasma oscillations to radio emissions, this would correspond well with the jump observed in the magnetic field. However, the level of oscillations in the peak wave amplitudes after day 182 makes it difficult to know for sure whether the ongoing activity is due to plasma oscillations or radio waves. The PWS on V2 no longer has the ability to transmit high-resolution waveform data; hence, only the coarse spectrum analyzer data are available. Nevertheless, the intense bursty intermissions almost certainly argue for the presence of the shock associated with this event.

Further evidence that the jump “sha” was a shock is that it was preceded by cosmic-ray intensity enhancements that began on day 163 of 2020 and lasted for roughly 7 days, as shown by Figure 7. “Shock spikes” were seen in both electron- and proton-dominated rates, with energies of ~ 3 –14 MeV and

~ 18 –70 MeV, respectively. Intensities of these shock-accelerated cosmic rays peaked to around 10% and 8% above background—twice the magnitude of analogous events seen by V1—possibly due to the larger-amplitude magnetic field at V2. Electron plasma oscillations followed the cosmic-ray enhancements, beginning around day 172, peaking from day 178 to day 180 and ending around day 194. The timing of these precursor events is captured in Figure 7 and is consistent with the “foreshock model” developed by Gurnett et al. (2013, 2015, 2021), as discussed above. This model was successfully used to account for particle and plasma energization in response to shocks seen at V1 (see also Kota & Jokipii 2017). In contrast, such short-lived precursor activity is conspicuously absent prior to each of the V1 pressure fronts (Rankin, private communication). Therefore, these newly reported observations at V2 support the interpretation that this third jump in B was, indeed, a shock.

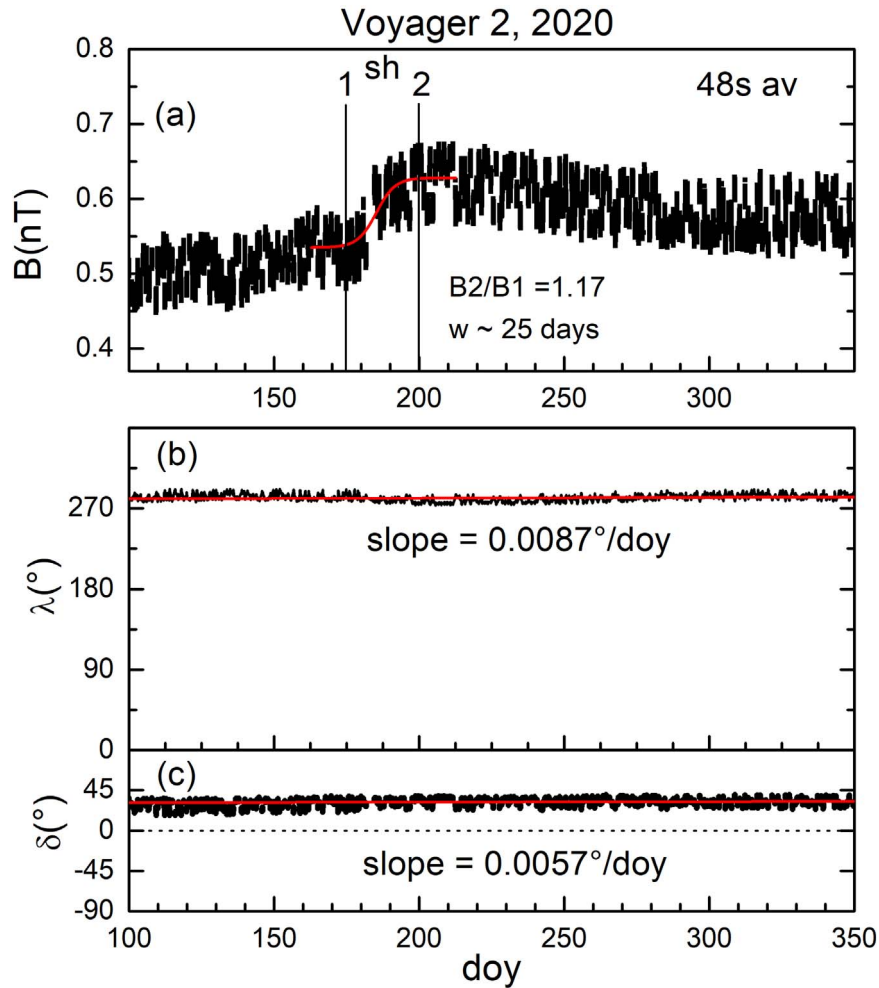


Figure 5. Panel (a) shows a jump in the 48 s averages of the magnetic field strength B (“sh”) in the V2 observations near 2020 \sim day 182. The jump began to move past V2 at the time indicated by the vertical line 1 and ended at the time shown by the vertical line 2. The jump in B moved past the spacecraft in ~ 25 days, and the size of the jump in B was $B_2/B_1 = 1.17$. Panels (b) and (c) show the azimuthal angle and elevation angle of the magnetic field, respectively. The slopes of the lines are $0.0087^\circ/\text{day}$ and $0.0057^\circ/\text{day}$, respectively.

The shock is shown in Figure 5, which is a plot of 48 s averages from day 100 to day 350. The shock occurred in the vicinity of \sim day 185, between the two vertical lines in Figure 5(a) labeled 1 and 2. A sigmoid fit to the magnetic field data plotted in red in Figure 5(a) shows that B increased by the ratio $B_2/B_1 = 1.17$ during an interval of $w \sim 25$ days. The large “width” w and long passage time of the shock have been explained theoretically by Mostafavi & Zank (2018a, 2018b) as the result of a collisional shock in which magnetic resistivity and viscosity produce a wide shock, in contrast to the collisionless shocks in the solar wind.

This observation of a shock at V2 near the heliopause, together with the observations of shocks near the heliopause observed by V1 (Gurnett et al. 2013; Burlaga & Ness 2014; Burlaga et al. 2021), confirms a prediction of Gurnett et al. (1993). They observed remotely a 2–3 kilohertz radio emission event that was detected by V1 and V2 in 1992 July. Gurnett et al. (1993) suggested that this event was generated at or near the heliopause by an interplanetary shock that originated during a period of intense solar activity in May and early June of 1999. Whang & Burlaga (1993) modeled the event as the result of a shock driven by a global merged interaction region (GMIR; Burlaga 1995).

A ramp in B was observed behind the shock in which the B decreased slowly from day ~ 200 to day ~ 280 , after which the decrease ended abruptly and B remained nearly constant until day 350, as shown in Figure 5. Panels (b) and (c) in Figure 5 show that the azimuthal angle and the elevation angle, respectively, were constant throughout the interval from day 100 through day 350.

Waves in each of the components of the magnetic field, observed before and after the shock “sha” that is indicated by the vertical line on 2020 day 182, are shown explicitly by the curves in each panel of Figure 8. This figure shows plots of points corresponding to 1 day averages of the components of \mathbf{B} ($-B_T$, B_N , and B_R) and B in panels (b), (c), (d), and (a), respectively. The mean values of the magnetic field strength and components preceding the shock were $B_{av1} = 0.509$ nT, $-B_{Tav1} = 0.427$ nT, $B_{Nav1} = 0.257$ nT, and $B_{Rav1} = 0.088$ nT in Figures 8(b), (c), and (d), respectively. The mean values B and components following the shock were $B = 0.595$ nT, $-B_{Tav2} = 0.489$ nT, $B_{Nav2} = 0.320$ nT, and $B_{Rav2} = 0.099$ nT. The points in Figure 9(a) prior to the shock show the difference between the successive of daily averages of $B = 0.509$ nT and the mean values $B_{av1}(t)$ plotted as a point for each daily observation measurement of B during the first half of the year. Similarly, the points on the right-hand side of Figure 9(a) show

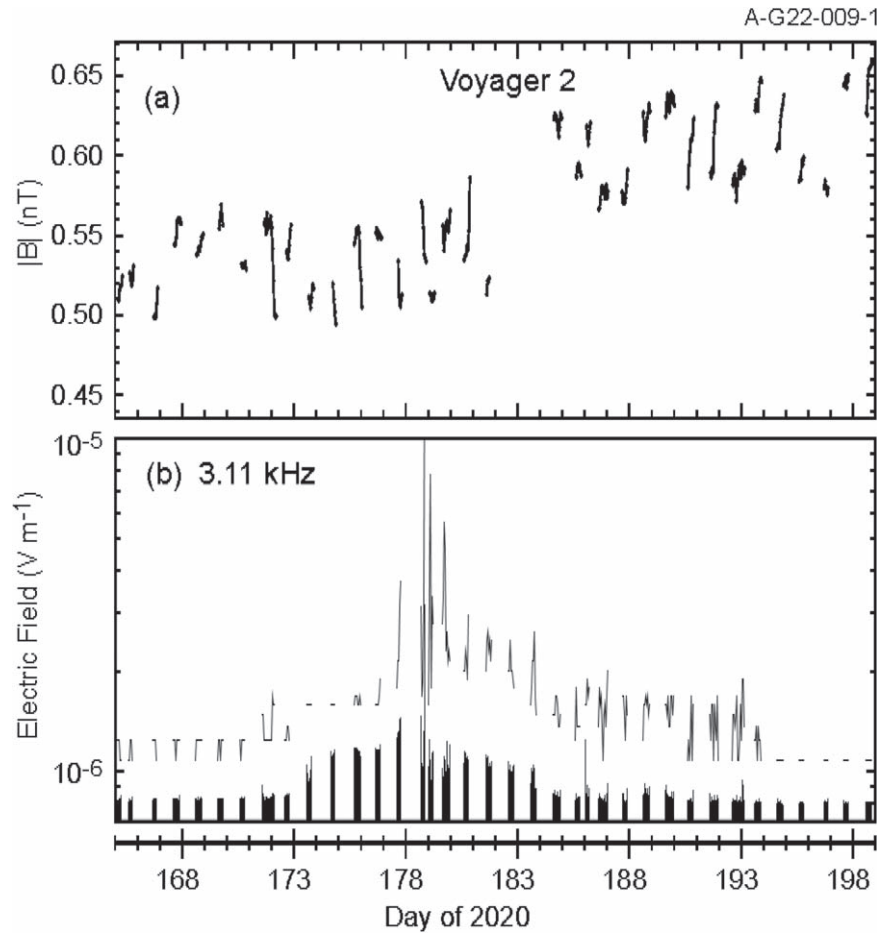


Figure 6. Panel (a) shows a close-up of the 48 s averages of B shown in Figure 5, together with the 3.11 kHz electric field measured by the PWS experiment on V2. The very pronounced spike just ahead of the jump in B shows the electric field associated with electron plasma oscillations. This observation is very strong evidence that the jump in B was a shock.

the differences between the post-shock daily averages of B and the corresponding mean value 0.595 nT, for each daily observation measurement of B . Panels (b), (c), and (d) show the corresponding plots for the components $-BT$, BN , and BR minus the respective mean values before and following the shock “sh.”

Now let us consider the waves, which were associated with deviations from the mean values of the components whose values are given in nT, measured by the SD of the 1 day averages. The waves are shown by the red curves, which are cubic fits to the points. The standard deviation of B and each component of \mathbf{B} increased behind the shock, as shown by Figure 8. Specifically, the standard deviation of the radial $BR(t)$ component before and after the shock was $SD = 0.026$ nT and $SD = 0.030$ nT, respectively. Likewise, for the $-BT$ component $SD = 0.017$ nT and $SD = 0.021$ nT and for the BN component $SD = 0.039$ nT and $SD = 0.045$ nT before and after the shock, respectively. In other words, the average standard deviations of the points corresponding to B and the components of \mathbf{B} were all larger during the interval following the shock than in the interval preceding it (Figure 8). This increase suggests that the waves were compressed and possibly augmented by the shock as they moved past it. Figure 8 shows that despite the changes in the mean values of the components of \mathbf{B} as a consequence of the jump in B , the direction of the magnetic field \mathbf{B} did not change across the shock.

The waves observed by V2 with the *smallest* amplitudes during 2020 (namely, $SD = 0.017$ nT before the shock and $SD = 0.021$ nT after it) were in the $-BT$ component. Longitudinal waves propagate near T -direction, within 25° of the average magnetic field in the VLISM. Thus, we have shown that, at a distance of 122.6–125.8 au (3.6–6.8 au beyond the heliopause), the amplitudes of the fluctuations observed before and after the shock in 2020 were smallest in the longitudinal BT direction.

On the other hand, we found that the *largest* fluctuations (measured by SD) were in the transverse BN and BR components. Specifically, ahead of the shock the transverse components BN and BR were the dominant components of the waves ($SD = 0.039$ and 0.026 nT), and the longitudinal $-BT$ component was the smallest component ($SD = 0.017$ nT). Behind the shock, the dominant components were again the transverse components BN and BR ($SD = 0.045$ and 0.030 nT), and the relatively weak longitudinal component was $-BT$ ($SD = 0.021$ nT). Thus, we observed primarily *transverse* waves near the shock at ~ 4 – 7 au from the heliopause.

This result confirms both the hypothesis of Burlaga et al. (2014) and the results observed by the V1 near the heliopause by Burlaga et al. (2018) that close to the heliopause the fluctuations in \mathbf{B} were observed to be longitudinal (because they were transmitted from the heliosheath) and beyond several au the fluctuations in \mathbf{B} are primarily transverse (Alfvénic).

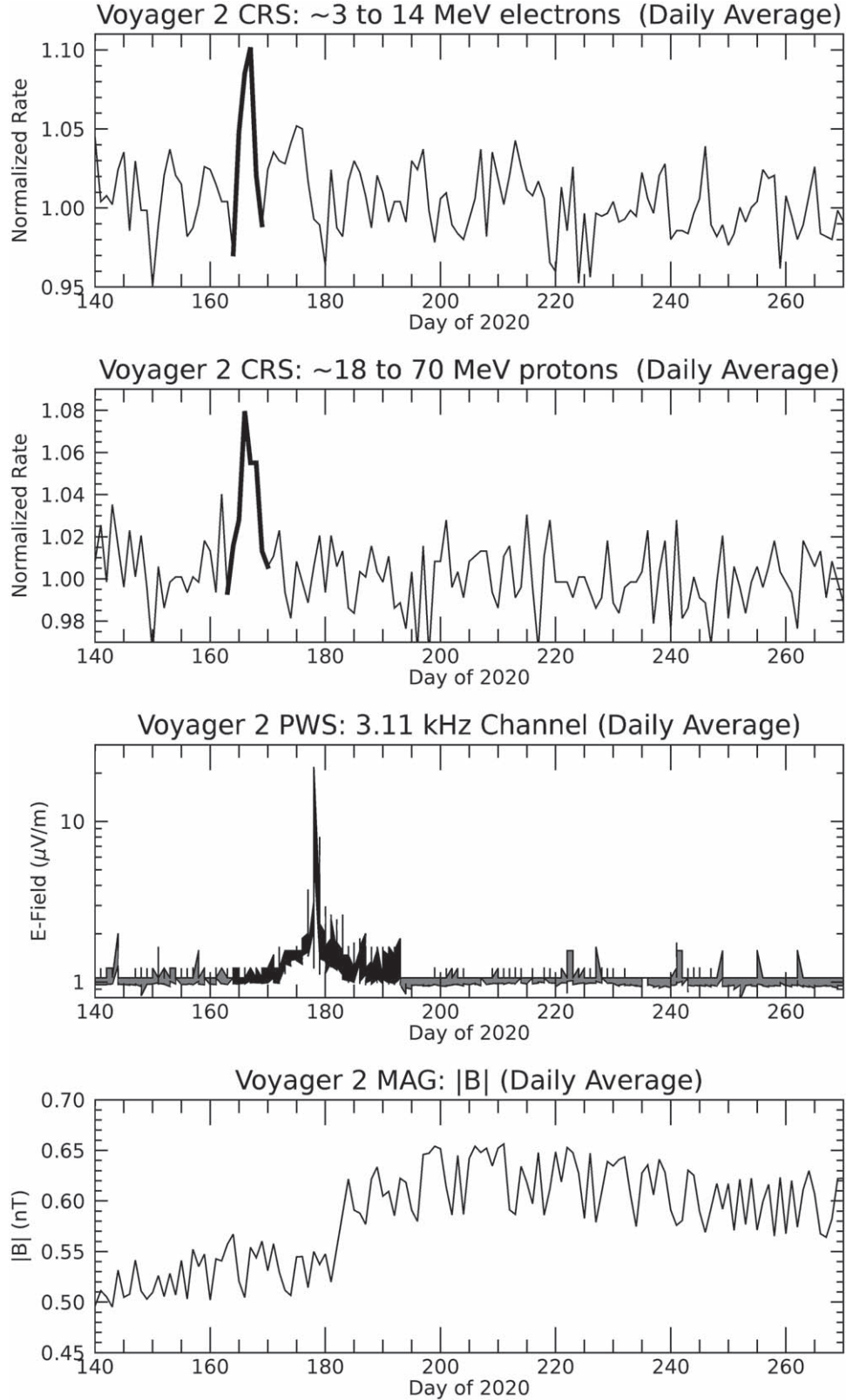


Figure 7. The top panel shows daily averages of ~ 3 to 14 MeV electrons measured by the Cosmic Ray Subsystem (CRS) instrument in V2. The panel beneath it shows observations of ~ 18 –70 MeV protons. The lower two panels show the electric field from the PWS experiment for the jump in the magnetic field discussed in Figure 6. It is clear that the particles producing the two peaks in the CRS observations were accelerated by the shock that produced the spike in electric field and the jump in B near day 180 of 2020.

A theory of this mode conversion process, in which a fast magnetosonic mode is converted to an incompressible Alfvén mode, was developed by Zank et al. (2019). Fast magnetosonic

waves undergo mode conversion via a three-wave interaction as they propagate in the approximately homogeneous VLISM, decaying into Alfvén waves and a zero-frequency Elsässer

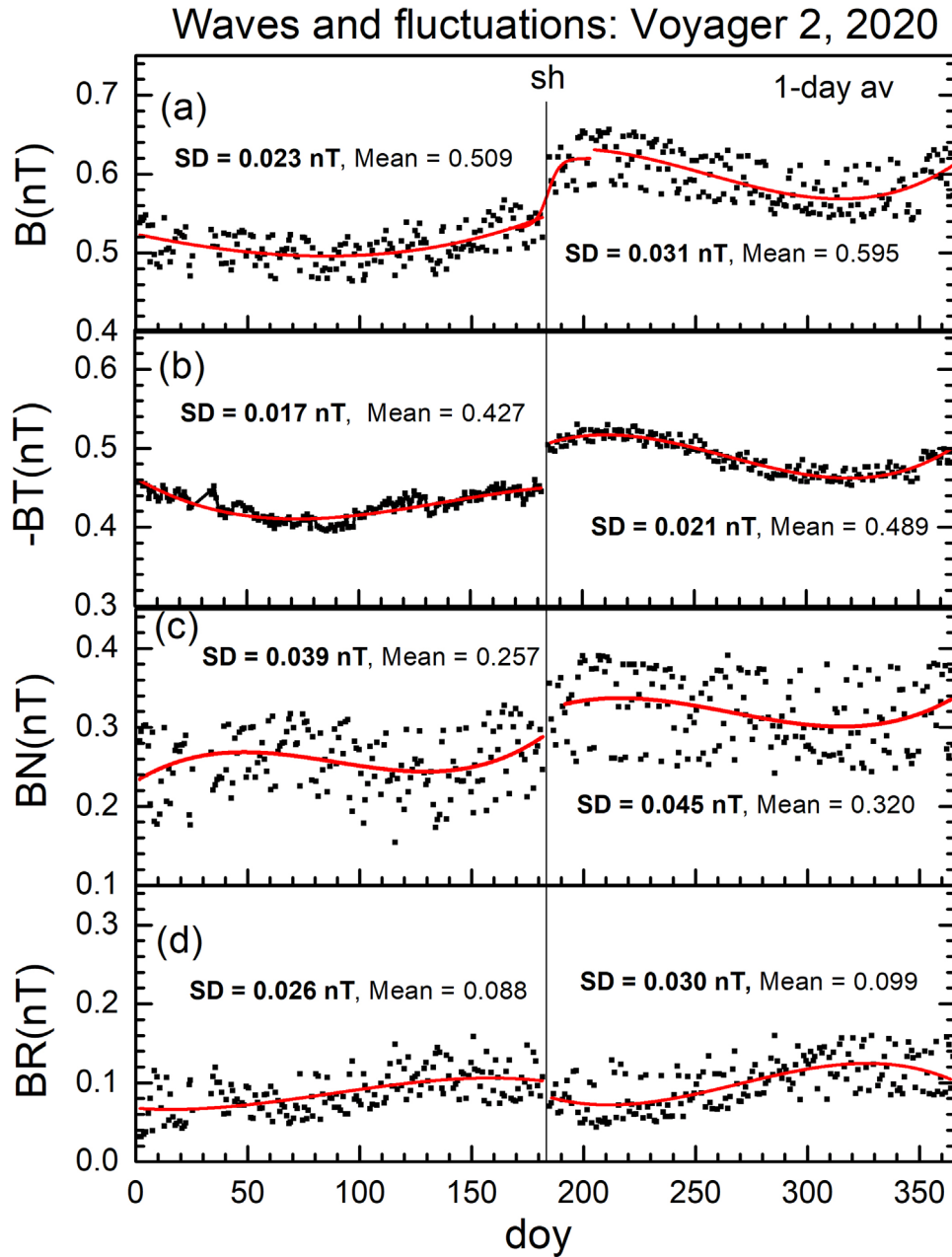


Figure 8. This figure shows that the jump in B at the shock on 2020 day 182 was primarily in the $-BT$ component of the magnetic field (panel (b)), but there were also changes in the BN (panel (c)) and BR components (panel (d)) as well. Wave-like features are seen in all of the components before and after the shock. The curves in these panels are cubic fits to the data points. The standard deviation of these waves was greater behind the shock than ahead of it, probably produced by shock compression. The largest waves, measured by the standard deviation, were in the transverse BN and BR components, indicating that the waves were primarily transverse waves.

vortex in the range of frequencies considered in this paper. They predicted that this conversion from compressible to incompressible fluctuations occurs within ~ 10 au of the heliopause, consistent with the observations at V2 discussed above and the observations at V1 by Burlaga et al. (2018).

3.4. Intermittency in the Magnetic Field Preceding and Following the Jump in B (“sh”) during 2020 at Voyager 2

In addition to the relatively long wavelength fluctuations described in the previous section, V2 observed small-scale intermittency in the VLISM (Burlaga et al. 2020b). In this section we show that intermittency was observed during 2020 in the VLISM at ~ 4 – 7 au from the heliopause. Intermittency of the

fluctuations of hourly averages of the magnetic field for 1 hr increments is found by plotting $\delta Bx = Bx(t+1 \text{ hr}) - Bx(t)$, where Bx refers to the magnetic field strength, B , and its components BR , BT , and BN . A plot of the intermittency of these quantities as a function of time, before and after the shock, is shown in Figure 9. Each panel shows the standard deviation of the intermittency and the kurtosis K of the hourly averages. The intermittency in a time series of $B(t)$ and its components can be recognized as “spikes” in the time series $\delta Bx(t)$. For example, if δBx increased from one point to a second point in 1 hr by an amount that significantly exceeds one standard deviation and then dropped back to a low value in the third point, the result is seen as a spike in the time series for $\delta Bx(t)$.

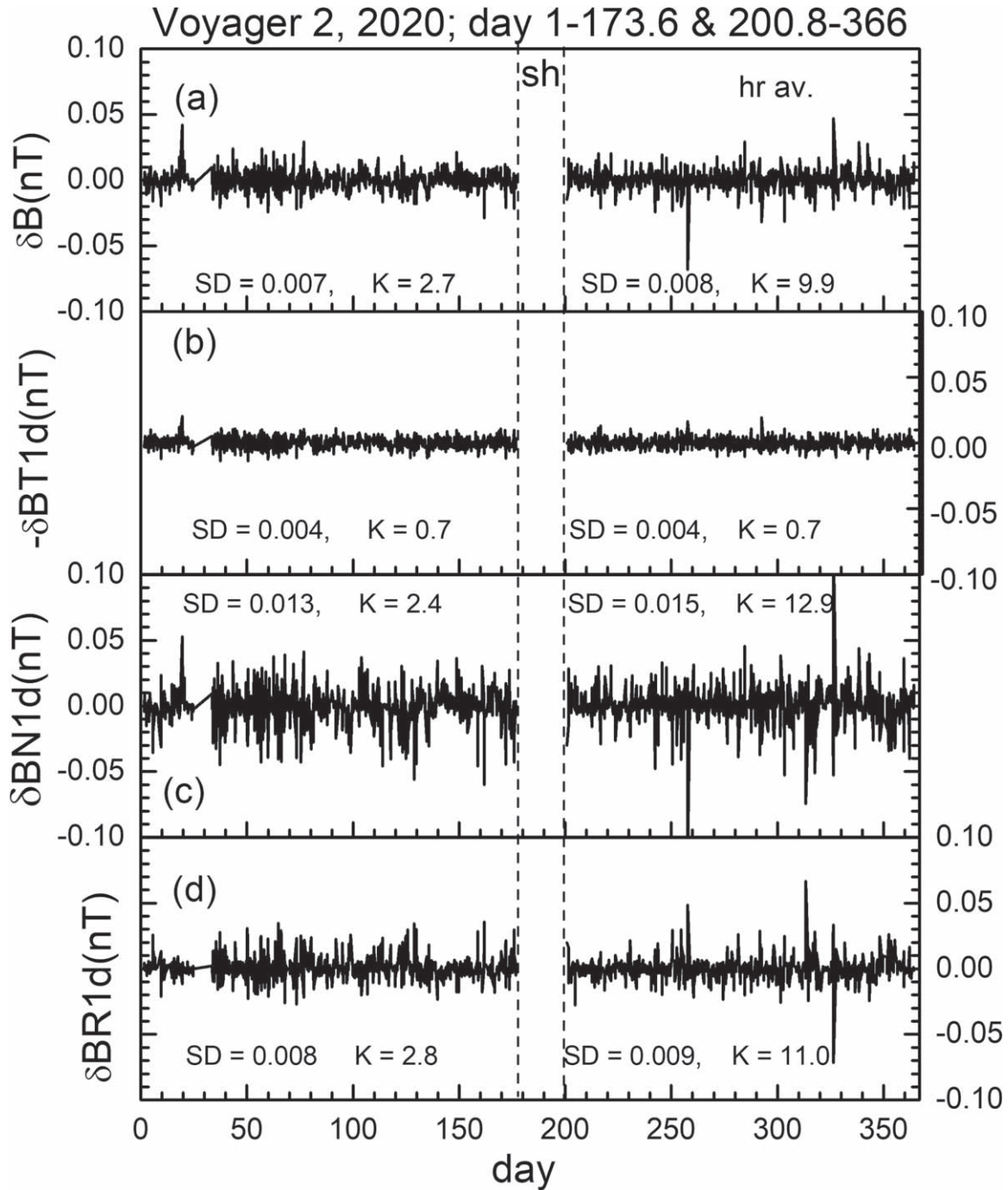


Figure 9. This plot shows the successive 1 hr increments of hourly averages of magnetic field strength and components. These increments give a measure of the intermittency of the magnetic fluctuations. There was no measurable intermittency in the longitudinal $-\delta BT1$ component shown in panel (b). The standard deviation was at the limit of measurements 0.004 nT before and after the shock. The kurtosis of this component before and after the shock was also very low, $K = 0.7$. The standard deviation of increments was significant in the $\delta BR1$ and the $\delta BN1$ components. The intermittency K in the transverse $\delta BR1$ and $\delta BN1$ components was relatively small before the shock, namely, $K = 2.8$ and $K = 2.4$, respectively. However, the intermittency K in the $\delta BR1$ and $\delta BN1$ components was large after the shock, namely, $K = 11.0$ and $K = 12.9$, respectively, suggesting that the intermittency was enhanced and perhaps created by the shock.

Visual inspection of the data from V2 during 2020 plotted in Figure 9 shows that the smallest spikes were in the longitudinal fluctuations $-\delta BT(t)$ (panel (b)), the intermediate spikes were in the radial fluctuations $\delta BR(t)$ (panel (d)), and the largest spikes were in the fluctuations $\delta BN(t)$ (panel (c)). Using the kurtosis K as a measure of the intermittency ($K = 0$ for a Gaussian distribution), one finds that the intermittency in the longitudinal fluctuations $-\delta BT(t)$ was $K = 0.7$ both before and after the shock, as shown in panel (b), indicating that

there was little or no intermittency in the BT component. Before the shock, the intermittency was small but significant for $\delta BN(t)$ (panel (c)) and for $\delta BR(t)$ (panel (d)), with $K = 2.4$ and $K = 2.8$, respectively. After the passage of the shock, however, the kurtosis was relatively large, namely, $K = 12.9$ for $\delta BN(t)$ (panel (c)) and $K = 11.0$ for $\delta BR(t)$ (panel (d)). Thus, the shock enhanced the intermittency by compression of turbulence plasma moving through it. Perhaps the shock itself was also a source of intermittency, which was presumably

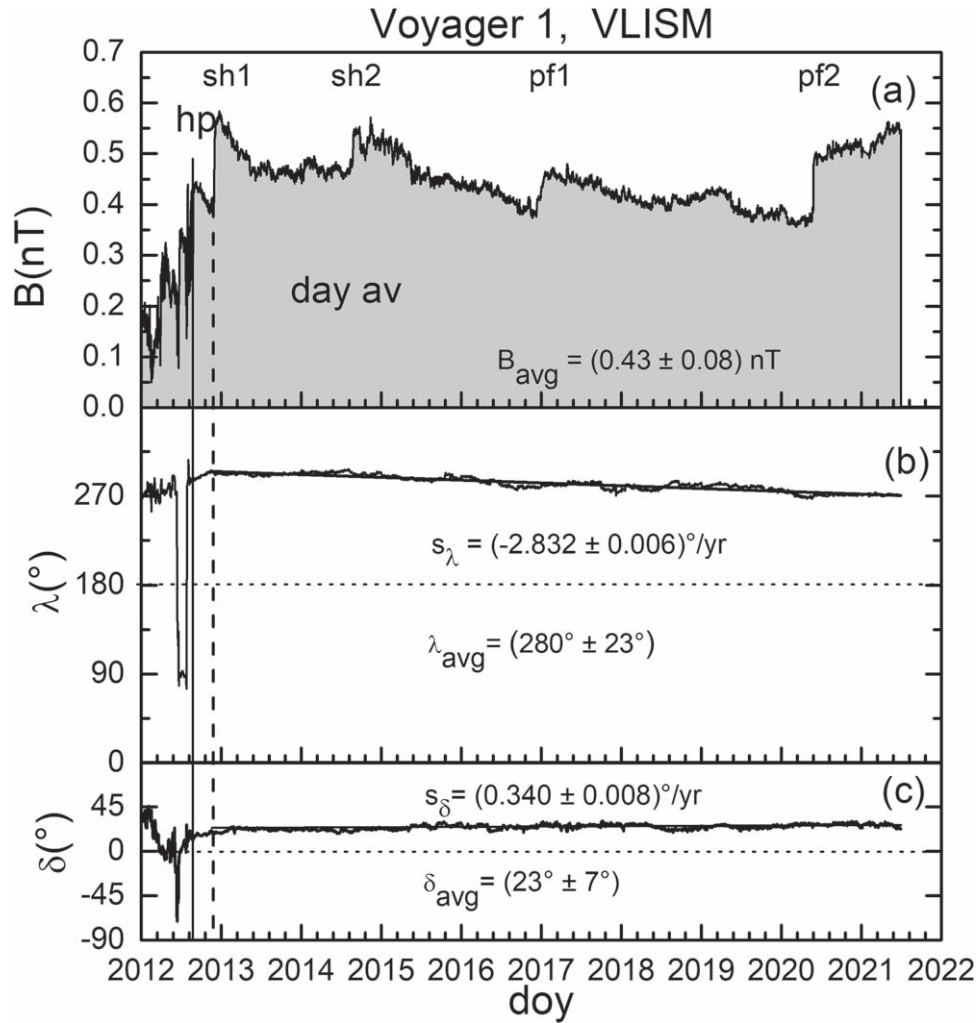


Figure 10. (a) A plot of the available measurements of the magnetic field strength and direction observed by V1 for a brief interval in the heliosheath before the heliopause crossing, as well as for 9 yr after crossing the heliopause. The dominant features are the familiar jump-ramp structures associated with shocks sh1 and sh2, as well as the pressure front pf1. A second large pressure front, pf2, occurred in 2020, but unlike the previous jumps, the magnetic field strength continued to increase at least 1 yr behind this jump! This long-term increase was unexpected and it is not understood. There was a slow linear decrease in λ (panel (b)) and a slow linear increase in δ (panel (c)) throughout the VLISM. No significant change in these angles was observed behind the jump pf2.

associated with turbulence generated by the shock that was propagating through the VLISM.

4. Voyager 1 Observations from 2012 through 2021.5

4.1. An Overview of the Voyager 1 Observations of the VLISM

Let us now turn to an overview of the V1 observations of the VLISM from 2012 through mid-2021, which are shown in Figure 10, from the time that V1 crossed the heliopause to the most recent data. Panels (b) and (c) show that the slow linear variation in the angles λ and δ with increasing distance continued with the same slopes, following the latest jump pf2. One can scarcely see the fluctuations about the linear slope in Figure 10. There were no changes in the angles associated with the passage of the jumps in B shown in panel (a).

Figure 10 includes an extension of an earlier figure showing the pressure front pf2 discussed by Burlaga et al. (2021) that ended on 2020 day 292. That paper emphasized that $B(t)$ was dominated by four maxima in B associated with four “jumps” in B , including the most recent jump pf2. It was shown that the first three jumps, the shocks sh1 and sh2 and the pressure front

(pf1), were followed by a relatively slow decay of B , compared to the short passage time of the shocks or the jump. It was natural to expect that the pressure front pf2 would also be followed by such a “ramp” of B , but the data needed to confirm that these were not available at the time that paper was published.

The components of the magnetic field and the magnitude B from 2012.0 to 2021.5 are shown in Figure 11. The top panel shows B versus time, as shown in Figure 10, but we also show pairs of dashed lines indicating the onset of a jump and the end of the ramp that follows the jump, for the events sh1, sh2, and pf1. Each of these jumps was followed by a decrease in B (the ramp) that ended abruptly at the time of a second dashed line that marks the end of the ramp. Thus, there are jump-ramp structures in Figure 11.

In addition, Figure 11 shows the jump pf2 in B in the VLISM during 2020. The very important and surprising thing about this jump is that B continued to *increase* for at least a year following the jump pf2, rather than decrease as observed behind the three earlier jumps! This increase in B was not anticipated, and it has no obvious explanation.

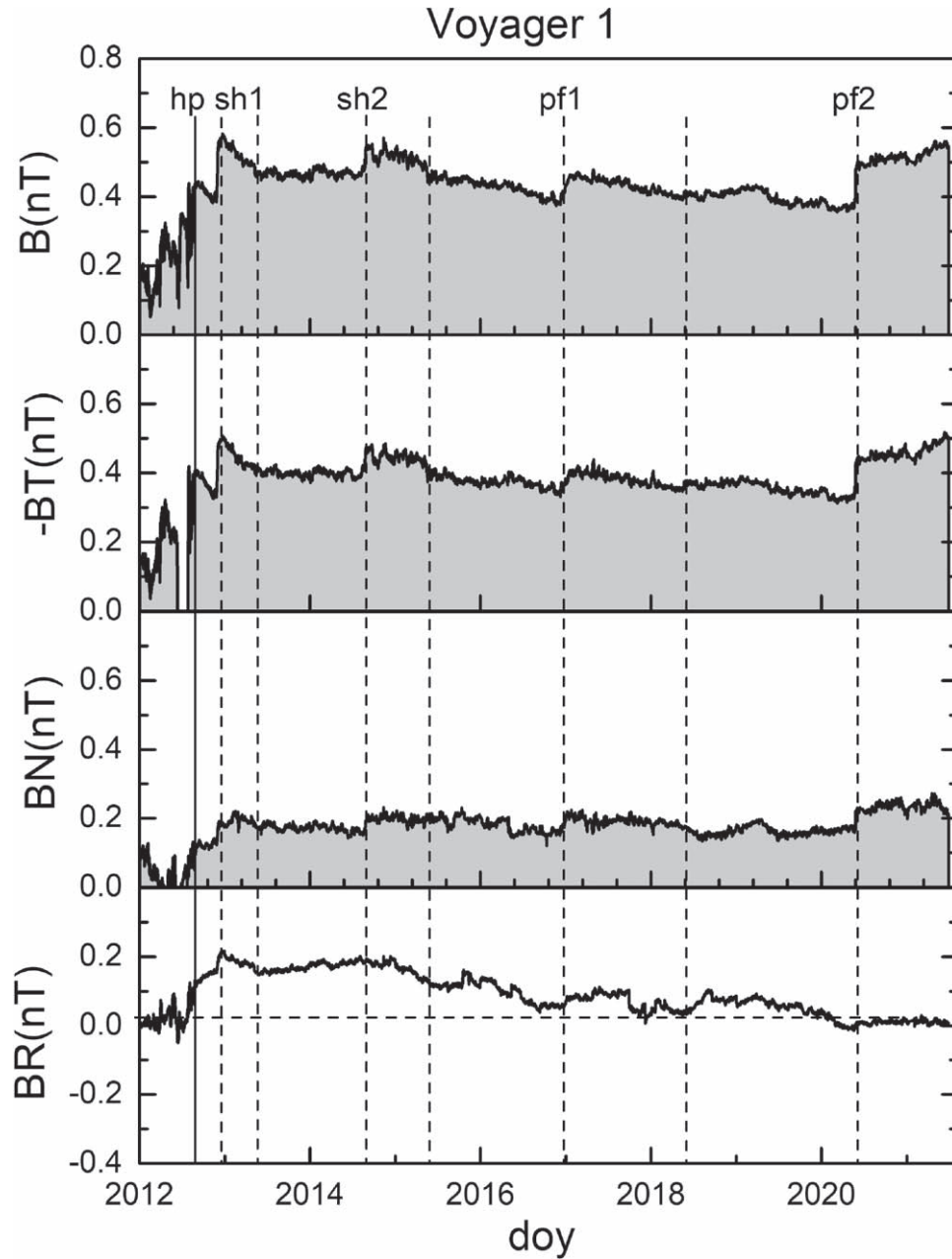


Figure 11. This figure shows B and components of \mathbf{B} observed by V1. The jump-ramp structures associated with sh1, sh2, and pf1 are indicated by the pairs of vertical dashed lines. The ramps are well defined only in the $-BT$ component. There is a continuing increase in B , BT magnitude behind pf2, which is also accompanied by an increase in BN .

4.2. Voyager 2 Observations of the Magnetic Fields Following pf2

In the remainder of this paper we discuss the prolonged increase in B following the jump pf2. This increase in B began on 2020.4 and continued to at least 2021.5 (the end of the current data set), as shown in Figure 12(a). The increase was more rapid near the end of the interval, as we discuss below. The increase in B was observed primarily in the longitudinal BT component (Figure 12(b)), but it can also be seen in the BN component (Figure 12(c)). The radial component of \mathbf{B} was very close to zero, while B was increasing following pf2 (Figure 12(d)).

The increase in B behind pf2 was nearly linear with a slope $s_B = (0.063 \pm 0.005) \text{ nT day}^{-1}$ before a data gap in 2021.0. After the gap, the slope of B increased more rapidly, with

$s_B = 0.123 \pm 0.060 \text{ nT day}^{-1}$ until 2021.5. The BR component contributed little to the increase in the slope of $B(t)$. The slope was $s_{BR} = 0.009 \pm 0.002 \text{ nT day}^{-1}$ before the gap and $s_{BR} = -0.012 \pm 0.004 \text{ nT day}^{-1}$ after the data gap until 2021.5. There was a significant decrease in the slope of BT , namely, $s_{BT} = -0.036 \pm 0.003 \text{ nT day}^{-1}$ before the gap and $s_{BT} = -0.151 \pm 0.006 \text{ nT day}^{-1}$ after the data gap, that contributed a significant increase in B . The slope of B was primarily in the BN component, namely, $s_{BN} = 0.060 \pm 0.009 \text{ nT day}^{-1}$ before the gap and $s_{BN} = 0.009 \pm 0.002 \text{ nT day}^{-1}$ after the data gap until 2021.5.

A closer look at these observations of the magnetic field is presented in Figure 13, where B and the components of \mathbf{B} on the ordinates are plotted on a scale that extends over 0.1 nT in increments of 0.02 nT. On this scale, considerable scatter of the

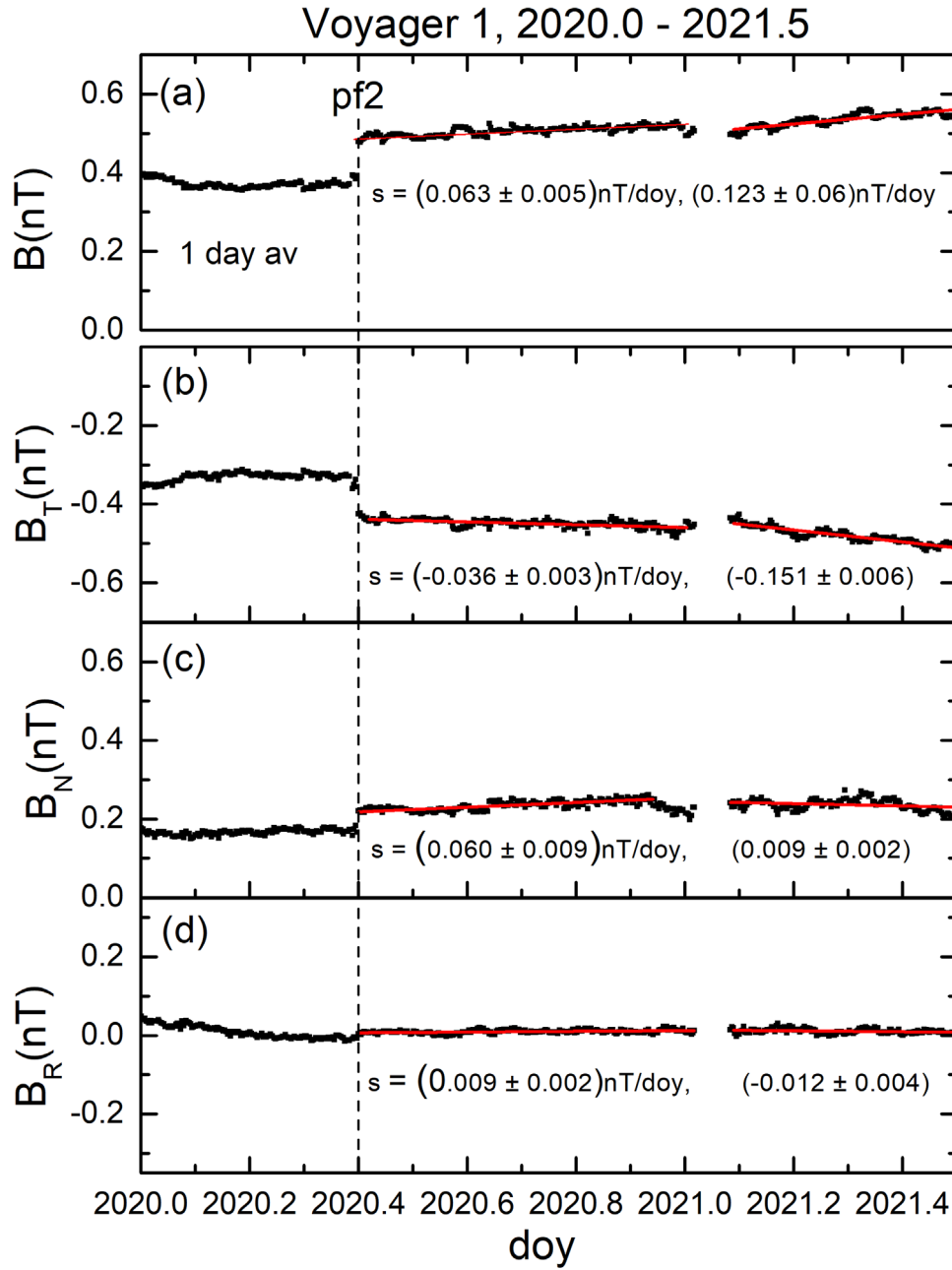


Figure 12. This is a higher-resolution plot of the jump pf2 showing the linear increase in B and components of B extending from 2020.4. This figure shows that this increase in the magnetic field strength and components BT and BN can be described by two lines, to the first approximation. The slopes of these lines are shown in each panel.

points is evident. Most of this scatter represents the uncertainty in the observations, which can be ± 0.02 nT in absolute terms. The solid curves in each of the four panels of Figure 13 are cubic fits to the observations, as is opposed to the two linear fits in each panel discussed in Figure 12. The component $BR(t)$ in Figure 13(d) was nearly constant at ~ 0.01 nT, which is consistent with zero within the uncertainties. The BN component was weakly parabolic, with an average of approximately 0.21 ± 0.01 nT. Thus, it is evident that the increasing B from 2020.4 to 2021.5 shown in Figure 13(a) was primarily determined by the longitudinal component BT . In particular, the plots of $B(t)$ in Figure 13(a) and $BT(t)$ in Figure 13(b) are nearly mirror images of one another.

Finally, a close-up of $B(t)$ observed by V1 at the end of the data set that we have been discussing, from 2021 day 30 to day

180, is plotted in Figure 14. Again, the scale was magnified by plotting the abscissa between 0.48 and 0.57 nT. One can see quasi-periodic oscillations in B , with an average period of approximately 30 days, which is close to the solar rotation period. Quasi-periodic oscillations with a somewhat lower period were also observed behind pf1 by Burlaga et al. (2019a), but the nature and origin of these waves have not been explained. Perhaps quasi-periodicity in this case is related to the tilt of the heliosphere current sheet (HCS) during the ascending phase of solar cycle (the Royal Observatory in Belgium; the new solar activity cycle⁹).

Since the density is high in the vicinity of the HCS and the tilt of the HCS might be near the latitude of V1, a pressure

⁹ ISILSO (sidc.be).

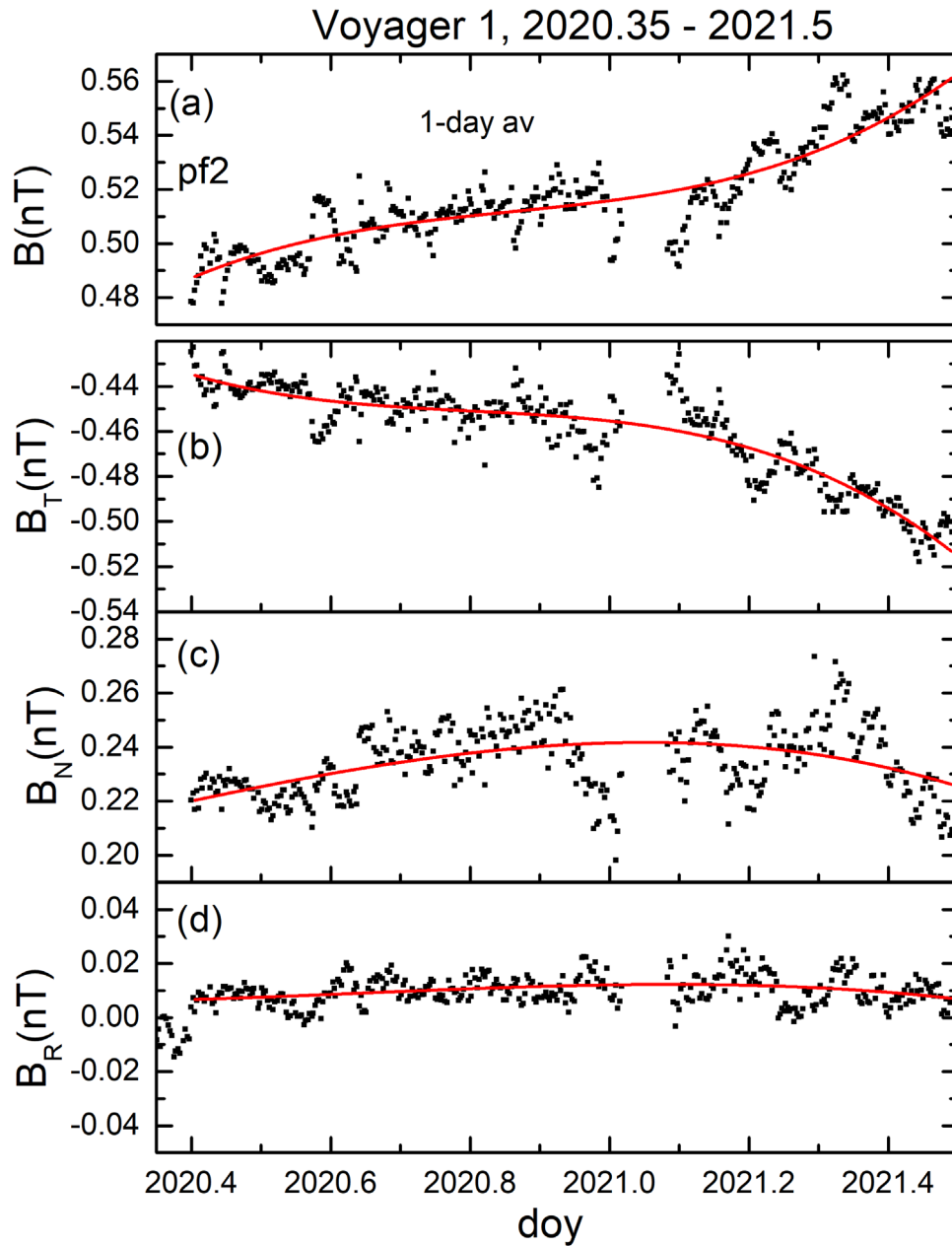


Figure 13. This is an amplified view of Figure 12, with a cubic fit to the observations, but the same range of values on the ordinate of each panel. (a) The increase in B is clearly associated primarily with the BT component (panel (b)). The BN component (panel (c)) can be described by a relatively flat parabola, and the BR component (panel (d)) is essentially constant.

pulse would hit the heliopause and pass through it for an extended time, when the HCS moves to or past the latitude of the spacecraft. If the latitude of the HCS moves significantly beyond the latitude of V1, it will return to lower latitudes as the solar cycle progresses and produce another pressure pulse. A similar phenomenon should occur in the southern hemisphere if the HCS might be observed by V2. This hypothesis and other studies of these observations should be explored using modeling techniques and future observations.

5. Summary and Discussion

Both the V1 and V2 spacecraft are now in the VLISM, moving north of the solar ecliptic plane and south of it, respectively. V1 crossed the heliopause on ~ 2012 August 25, at 121.58 au, and on 2022 January 1 it was at 155.00 au,

33.42 au from the heliopause. V2 crossed the heliopause on ~ 2018 November 5 at 119.0 au, and on 2022 January 1 it was at 129 au, 10 au from the heliopause.

V2 observed predominantly longitudinal waves in the magnetic field when it crossed the heliopause, and it observed transverse (Alfvén) waves several au beyond it. This confirms the existence of a mode conversion process in the region between the heliopause and ~ 10 au beyond, which was observed by V1 (Burlaga et al. 2018). Since the V2 observations were made at significantly different latitudes and longitudes than V1, they demonstrate that the mode conversion is a characteristic of a very extensive region associated with the heliopause that persists over a long interval of time.

V2 observed a jump in B (pfb) followed by a ramp in 2019. The magnetic field strength increased by $B2/B1 = 1.11$, which

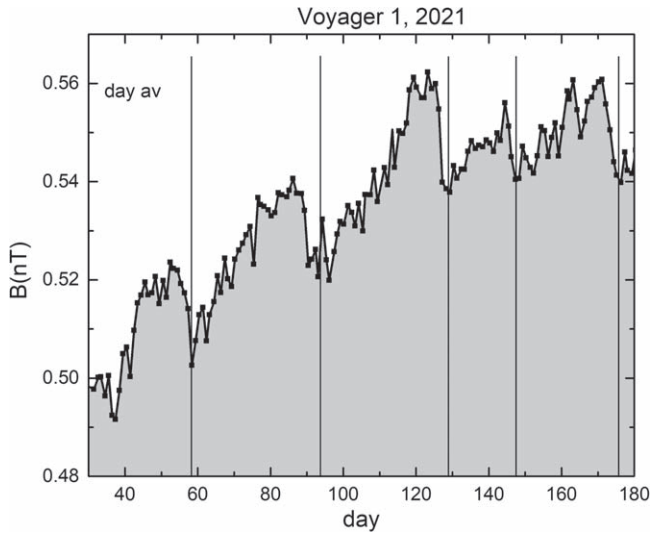


Figure 14. This is a further amplified plot of B of Figure 13 from day 30 to day 180 of 2021. There is a quasi-periodic structure of B with a period of approximately 30 days, which is close to the solar rotation period.

is the range of the three jumps in B observed previously by V1. The width (passage time) of this jump was ~ 7 days, and the ramp persisted for ~ 90 days. There was no change in direction of \mathbf{B} across the jump.

A second jump/ramp structure in B was observed by V2 in association with a shock that occurred near the middle of a 2020 (\sim day 182). This shock “sha” was identified by the electron plasma oscillations that preceded it and by the fact that it accelerated cosmic-ray protons (~ 18 – 70 MeV) and electrons (~ 3 – 14 MeV) to $\sim 10\%$ above their typical intensity levels. The jump in B across the shock was $B_1/B_2 = 1.17$, and the width (passage time) of the shock was ~ 25 days, indicating that it was not a collisionless shock. Increasingly strong magnetic fields were observed for at least ~ 150 days.

During 2020, prior to the shock observed at 2020.435, there was a wave-like structure at V2 in $B(t)$ and each of the components of $\mathbf{B}(t)$ that could be described with cubic polynomials. The same is true of the observations behind the shock, until at least the end of 2020. The dominant components of the waves were the transverse BN and BR components on both sides of the shock. The standard deviations were equal to 0.039 and 0.026 nT, respectively, before the shock, and they were 0.045 and 0.030 nT after the passage of the shock. The larger amplitudes of waves behind the shock were presumably produced by compression at the shock. The standard deviation of the longitudinal BT component was only 0.017 and 0.021 nT before and after passage of the shock, respectively. The larger-amplitude waves observed in the BN and BR components ahead of the shock and behind it were transverse (Alfvén) waves.

The transverse waves are in contrast to the longitudinal waves that were observed by V2 when it was closer to the heliopause. Thus, a wave conversion process occurred between the heliopause (near which the waves were longitudinal) and ~ 10 au (beyond which the waves were transverse). A similar wave conversion was observed by V1, as referenced above. Since V1 is widely separated from V2, our new observations show that this process is a general feature observed near the heliopause, in latitude, longitude, and time of the solar cycle. A

physical mechanism for this wave conversion process was proposed by Zank et al. (2019).

V2 also observed the intermittency on a scale of 1 hr during 2020. The intermittency was small in the longitudinal fluctuations of the BT component and larger in the transverse fluctuations of the BN and BR components. The intermittency, measured by the kurtosis K , was small ($K = 0.7$) in the longitudinal component, both before and after the shock.

V1 observations, made during 2020 and the first half of 2021, are also discussed in this paper. V1 observed a large jump in B (comparable to that associated with the first shock observed in the VLISM) associated with a pressure front pf2 far from the Sun (Burlaga et al. 2021). However, unlike previous jumps in B , the observation of pf2 on 2020.4 was followed by an extraordinary increase in the magnetic field that persisted until at least a year later, 2021.4! To first approximation, the increasing magnetic field strength can be represented as two linear increases in B . The first increase had the slope of 0.063 nT/day, and the second increase was more rapid, at 0.123 nT/day. Closer examination shows that the increase in B can be represented as a cubic polynomial. The increase in B was primarily in the BT component, and there was a smaller parabolic variation in the BN component. The radial component was essentially constant and < 0.01 nT, which is in the noise. Near the end of the increase in the V1 observations of B , between 2021 day 30 and day 180, B oscillated quasi-periodically with the period near 30 days while B was increasing. Since this is close to the solar rotation period, it suggests that the observations were driven by the Sun, perhaps by increasing solar activity or variations in the mobile hemispheric current sheet and associated dense flows. However, we cannot exclude the effects of the VLISM.

L.F.B. was supported by NASA contract 80GSFC19C0012. D.B.B. was supported by the Voyager project under a cooperative agreement support with TRIDENT.

ORCID iDs

L. F. Burlaga <https://orcid.org/0000-0002-5569-1553>
 L. K. Jian <https://orcid.org/0000-0002-6849-5527>
 W. Kurth <https://orcid.org/0000-0002-5471-6202>
 J. Park <https://orcid.org/0000-0002-8989-4631>
 J. Rankin <https://orcid.org/0000-0002-8111-1444>
 A. Szabo <https://orcid.org/0000-0003-3255-9071>

References

- Behannon, K., Acuna, M. H., Burlaga, L. F., et al. 1977, *SSRv*, **21**, 235
- Berdichevsky, D. B. 2009, White Paper, Voyager Mission, Detailed processing of weak magnetic fields I—Constraints to the uncertainties of the calibrated magnetic field signal in the Voyager missions, https://vgrmag.gsfc.nasa.gov/Berdichevsky-VOY_sensor_opu090518.pdf
- Berdichevsky, D. B. 2015, Voyager Mission, Detailed processing of weak magnetic fields; II—Update on the cleaning of Voyager magnetic field density B with MAGCALs, v11/7/2015
- Burlaga, L. F. 1995, *Interplanetary Magnetohydrodynamics* (Oxford: Oxford Univ. Press)
- Burlaga, L. F., Florinski, V., & Ness, N. F. 2015, *ApJL*, **804**, L31
- Burlaga, L. F., Florinski, V., & Ness, N. F. 2018, *ApJ*, **854**, 20
- Burlaga, L. F., Florinski, V., Ness, N. F., & Heerikhuisen, J. 2014, *ApJ*, **792**, 134
- Burlaga, L. F., Kurth, W. S., Gurnett, D. A., et al. 2021, *ApJ*, **911**, 61
- Burlaga, L. F., & Ness, N. F. 2014, *ApJL*, **795**, L19
- Burlaga, L. F., & Ness, N. F. 2016, *ApJ*, **829**, 134
- Burlaga, L. F., Ness, N. F., Berdichevsky, D. B., et al. 2019a, *ApJ*, **877**, 31
- Burlaga, L. F., Ness, N. F., Berdichevsky, D. B., et al. 2019b, *NatAs*, **3**, 1007
- Burlaga, L. F., Ness, N. F., Berdichevsky, D. B., et al. 2020a, *ApJ*, **160**, 40

- Burlaga, L. F., Ness, N. F., Berdichevsky, D. B., et al. 2020b, *ApJL*, **901**, L2
- Burlaga, L. F., Ness, N. F., Gurnett, D. A., & Kurth, W. S. 2013a, *ApJL*, **778**, L3
- Burlaga, L. F., Ness, N. F., & Stone, E. C. 2013b, *Sci*, **341**, 147
- Fermo, R. L., Pogorelov, N. V., & Burlaga, L. F. 2015, *JPhCS*, **642**, 012008
- Gurnett, D. A., & Kurth, W. S. 2019, *NatAs*, **3**, 1024
- Gurnett, D. A., Kurth, W. S., Allendorf, S. C., & Poynter, R. L. 1993, *Sci*, **262**, 199
- Gurnett, D. A., Kurth, W. S., Burlaga, L. F., & Ness, N. F. 2013, *Sci*, **341**, 1489
- Gurnett, D. A., Kurth, W. S., Stone, E. C., et al. 2015, *ApJ*, **809**, 121
- Gurnett, D. A., Kurth, W. S., Stone, E. C., et al. 2021, *ApJ*, **161**, 11
- Holzer, T. E. 1989, *ARA&A*, **27**, 199
- Karmesin, S. R., Liewer, P. C., & Brackbill, J. U. 1995, *GeoRL*, **78**, 53
- Kim, T. K., Pogorelov, N. V., & Burlaga, L. F. 2017, *ApJL*, **843**, 32
- Kota, J., & Jokipii, J. R. 2017, *ApJ*, **839**, 126
- Krimigis, S. M., Decker, R. B., Roelof, E. C., et al. 2013, *Sci*, **341**, 144
- Krimigis, S. M., Decker, R. B., Roelof, E. C., et al. 2019, *NatAs*, **3**, 997
- McComas, D. J., Bzowski, M., Frisch, P., et al. 2010, *JGRA*, **115**, A09113
- Mostafavi, P., & Zank, G. P. 2018a, *ApJL*, **854**, L15
- Mostafavi, P., & Zank, G. P. 2018b, *JPhCS*, **1100**, 012018
- Parker, E. N. 1958, *ApJ*, **128**, 664
- Parker, E. N. 1961, *ApJ*, **134**, 20
- Pogorelov, N. V., Borovikov, S. N., Zank, G. P., & Ogino, T. 2009, *ApJ*, **696**, 1478
- Pogorelov, N. V., Fichtner, H., Czechowski, A., et al. 2017a, *SSRv*, **212**, 193
- Pogorelov, N. V., Heerikhuisen, J. R., Burlaga, L. F., Gurnett, D. A., & Kurth, W. S. 2017b, *ApJ*, **845**, 9
- Richardson, J. D., Belcher, J. W., Garcia-Galindo, P., & Burlaga, L. F. 2019, *NatAs*, **3**, 1019
- Richardson, J. D., Wang, C., Liu, Y. D., et al. 2017, *ApJ*, **834**, 190
- Stone, E. C., Cummings, A. C., Heikkilä, B. C., & Lal, N. 2019, *NatAs*, **3**, 1013
- Stone, E. C., Cummings, A. C., McDonald, F. B., et al. 2013, *Sci*, **341**, 150
- Wang, C., & Belcher, J. W. 1999, *JGR*, **104**, 549
- Washimi, H., Tanaka, T., & Zank, G. P. 2017, *ApJL*, **846**, L9
- Washimi, H., Zank, G. P., Hu, Q., et al. 2011, *MNRAS*, **416**, 1475
- Whang, Y. C., & Burlaga, L. F. 1993, *JGR*, **98**, 15221
- Zank, G. P. 1999, *SSRv*, **89**, 413
- Zank, G. P. 2015, *ARA&A*, **53**, 449
- Zank, G. P., Du, S., & Hunana, P. 2017, *ApJ*, **842**, 114
- Zank, G. P., & Müller, H.-R. 2003, *JGRA*, **108**, 1240
- Zank, G. P., Nakanotani, M., & Webb, G. M. 2019, *ApJ*, **887**, 116
- Zhao, L.-L., Zank, G. P., & Burlaga, L. F. 2020, *ApJ*, **900**, 166